

# Reconstructing the spatial structure of quantum correlations

Allen Scheie,<sup>1</sup> Pontus Laurell,<sup>2</sup> Elbio Dagotto,<sup>2,3</sup> D. Alan Tennant,<sup>2</sup> and Tommaso Roscilde<sup>4</sup>

<sup>1</sup>*MPA-Q, Los Alamos National Laboratory, Los Alamos, NM 87545, USA*

<sup>2</sup>*Department of Physics and Astronomy, University of Tennessee, Knoxville, Tennessee 37996, USA*

<sup>3</sup>*Materials Science and Technology Division, Oak Ridge National Laboratory, Oak Ridge, Tennessee 37831, USA*

<sup>4</sup>*Univ Lyon, ENS de Lyon, CNRS, Laboratoire de Physique, F-69342 Lyon, France*

(Dated: June 21, 2023)

Quantum correlations are a fundamental property of quantum many-body states. Yet they remain experimentally elusive, hindering certification of genuine quantum behavior, especially in quantum materials. Here we show that the momentum-dependent dynamical susceptibility measured via inelastic neutron scattering enables the systematic reconstruction of quantum correlation functions, which express the degree of quantum coherence in the fluctuations of two spins at arbitrary mutual distance. Using neutron scattering data on the compound  $\text{KCuF}_3$  — a system of weakly coupled  $S = 1/2$  Heisenberg chains — and of numerically exact quantum Monte Carlo data, we show that quantum correlations possess a radically different spatial structure with respect to conventional correlations. Indeed, they exhibit a new emergent length of quantum-mechanical origin — the quantum coherence length — which is finite at any finite temperature (including when long-range magnetic order develops). Moreover, we show theoretically that coupled Heisenberg spin chains exhibit a form of quantum monogamy, with a trade-off between quantum correlations along and transverse to the spin chains. These results highlight real-space quantum correlators as an informative, model-independent means of probing the underlying quantum state of real quantum materials.

Quantum superpositions are among the most profound and fascinating phenomena in nature. They give rise to a variety of quantum correlations, including entanglement [1] and Bell nonlocality [2], both considered resources in quantum information processing. Such quantum correlations have been experimentally demonstrated in systems of few degrees of freedom sufficiently isolated from their environment, such as photons [3, 4], atoms [5–7], and superconducting circuits [8, 9]. However, quantum materials—which host a wealth of exotic physical states [10]—sit at the opposite end of the many-body spectrum. They contain Avogadro numbers of quantum-mechanical degrees of freedom, interacting strongly and locally, so that their physics is very sensitive to the underlying system geometry. Certifying the quantum superposition nature of such systems, and understanding effects of geometry and dimensionality of interactions on quantum correlations, represent grand challenges for quantum condensed matter physics, as well as new opportunities to understand the role of quantum mechanics in macroscopic systems.

Fortunately, quantum information offers powerful tools for probing quantum superpositions in generic systems in the form of coherence measures [11–14]. Here we focus on observable-based measures, which probe coherences of a quantum state when represented on the eigenbasis of an observable, i.e. the non-commutativity between the observable and the density matrix. Coherences manifest themselves in interferometric experiments [13], and provide the basis of the metrological sensitivity of a quantum state. Yet interferometry is rarely accessible in the solid-state context; nor is the density matrix itself. However, recent works [15–17] have related quantum coherence measures for quantum states in thermal equilibrium to linear response functions, which are directly accessible to solid-state spectroscopic techniques (such as light scattering, AC magnetometry, or inelastic neutron scattering). This link allowed neutron scattering experiments

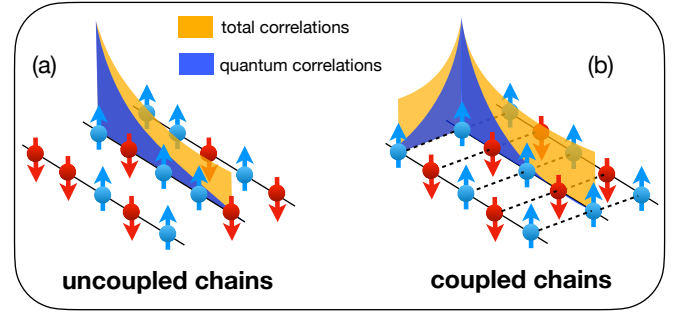


**FIG. 1. Total vs. quantum correlations in  $S = 1/2$  Heisenberg chains.** (a) Uncoupled 1D chains, and (b) chains subject to interchain coupling. Total and quantum correlations are widely different at any finite temperature. Whereas total correlations are enhanced in all directions when coupling the chains at fixed temperature, quantum correlations are redistributed spatially (at low temperatures), due to an effective form of monogamy (i.e. mutual exclusion).

on quantum magnets [18, 20, 64] to reconstruct their quantum Fisher information (QFI) [13, 21]. Measurements of QFI associated with order parameters have, in turn, led to estimates of the entanglement depth — i.e. a lower bound to the minimal number of entangled degrees of freedom in a multipartite entangled state — in the low-temperature phase of low-dimensional magnets, such as spin chains and triangular anti-ferromagnets [20, 22, 64].

Although the entanglement depth revealed by QFI is important, it does not reveal the spatial organization of quantum correlations. In this work we show that a Fourier analysis of the linear response function measured in neutron scattering, reweighted by an appropriate quantum filter function, allows one to extract the full spatial structure of quantum correlations in a model-free manner, applicable to arbitrarily complex systems. Importantly, such analysis can reveal surprising

and new information, even for very well-studied models and materials.

Quantum correlation functions can be generally defined as the difference between two types of correlations that are classically equivalent, and that coincide quantum-mechanically only when the correlated observables commute with the state: *e.g.* the statistical correlations of two fluctuating observables, and the response of an observable to a field coupling to the other observable. This latter notion coincides with the *quantum covariance* introduced in Ref. [23]; but related quantities (connected to QFI or the Wigner-Yanase-Dyson skew information (SI) [24], see Methods section) can also be defined.

Making use of neutron scattering data on the  $S = 1/2$  Heisenberg antiferromagnetic chain system  $\text{KCuF}_3$  [25, 26, 64] and quantum Monte Carlo (QMC) simulations, we show that these quantum correlation functions share a common spatial structure; and, unlike the ordinary correlation function, they exhibit an exponential decay at all finite temperatures, with an emergent quantum coherence length [23] which differs substantially from the ordinary correlation length. We provide therefore a clear experimental observation of the short-range nature of quantum correlations at finite temperature, in agreement with recent numerical and analytical results [17, 23, 27]. We also show numerically that weakly coupled antiferromagnetic chains at low temperature exhibit stronger quantum correlations at short range than strongly coupled chains, due to an effective form of “monogamy” (i.e. mutual exclusion) of quantum correlations; see Fig. 1 for a sketch summarizing the main results.

*Theory of quantum correlation functions.*—For a lattice quantum system, we consider local Hermitian bounded operators  $O_i$ , with  $i$  the lattice site index; and introduce their sum building up the extensive observable  $O = \sum_i O_i$ . We then consider the two-site dynamical susceptibility  $\chi''_{O_i, O_j}(\omega)$  [28], expressing the out-of-phase variation of the expectation value of  $O_i$  in response to a periodic field oscillating at frequency  $\omega$  and coupling to  $O_j$ . Its mathematical expression reads  $\chi''_{O_i, O_j}(\omega) = -\int dt/\hbar e^{-i\omega t} \langle [O_i(t), O_j(0)] \rangle$ , where  $\langle \dots \rangle = \text{Tr}[\dots]\rho$  represents the thermal equilibrium average at temperature  $T$  when  $\rho = e^{-\beta H}/\mathcal{Z}$ , with  $\beta = (k_B T)^{-1}$ ,  $H$  the system Hamiltonian, and  $\mathcal{Z}$  the partition function. A family of quantum correlation functions can then be related to the two-site dynamical susceptibility via an integration over frequency, weighted by an appropriate quantum filter function  $h(\beta\hbar\omega)$ ,

$$C[O_i, O_j; h, \rho] = \frac{1}{\pi} \int_0^\infty d(\hbar\omega) h(\beta\hbar\omega) \chi''_{O_i, O_j}(\omega). \quad (1)$$

For  $C$  to be a well-defined measure of quantum coherence, the function  $h(x)$  must satisfy basic mathematical properties [29–32], namely  $h(x) \sim x$  when  $x \rightarrow 0$ , and  $h(x \rightarrow \infty) = 1$ ; in this way it acts a high-pass filter for frequencies  $\hbar\omega \gg k_B T$ , associated with excitation modes behaving quantum-mechanically at temperature  $T$ . Summing Eq. (1) over the spatial indices yields a quantum coherence measure associated with the observable  $O$ ,  $I[O; h, \rho] = \sum_{ij} C[O_i, O_j; h, \rho]$ .

In this work we focus mainly on the quantum covariance,  $\text{Cov}_Q$ , [17, 23] given by the filter function  $h_{\text{Var}_Q}(x) = \coth x - 1/x$ ; whose sum over spatial indices reconstructs the quantum variance,  $\text{Var}_Q(O; \rho)$  [16]. This definition corresponds to the difference between static correlations and static response functions [16, 23], and consequently quantum variance and covariance can be calculated efficiently with QMC. Similar quantum correlation functions (corresponding to different filters) can be defined in the form of the quantum Fisher information matrix (QFIM) [33] and the skew information matrix (SIM), whose respective sums reconstruct the QFI and the SI [24]; see Methods for their mathematical definitions.

*Quantum correlation functions from neutron scattering.*—Inelastic neutron scattering gives access to the dynamical structure factor  $S(\mathbf{k}, \omega)$ , related to the momentum-dependent dynamical susceptibility via the fluctuation-dissipation theorem  $\chi''(\mathbf{k}, \omega) = \pi(1 - e^{-\hbar\omega\beta})S(\mathbf{k}, \omega)$  [34], where  $\chi''_O(\mathbf{k}, \omega) = -\int dt/\hbar e^{-i\omega t} \langle \{O_{\mathbf{k}}(t), O_{-\mathbf{k}}(0)\} \rangle$  and  $O_{\mathbf{k}} = N^{-1/2} \sum_i e^{i\mathbf{k} \cdot \mathbf{r}_i} O_i$  is the Fourier transform of the  $O_i$  operators for a lattice with  $N$  sites. If  $S(\mathbf{k}, \omega)$  is measured across the full Brillouin zone, its inverse Fourier transform allows one to reconstruct the two-site dynamical susceptibility, and calculate the quantum correlation functions.

To test this idea, we use the neutron scattering data reported in Ref. [35] for  $\text{KCuF}_3$ ; see Methods for details. This material is an ideal approximation to a system of coupled Heisenberg  $S = 1/2$  chains [26, 36]

$$H = J \sum_{\langle ij \rangle: \text{chains}} \mathbf{S}_i \cdot \mathbf{S}_j + J_\perp \sum_{\langle lm \rangle: \text{inter}} \mathbf{S}_l \cdot \mathbf{S}_m \quad (2)$$

where  $\mathbf{S}_i$  is a  $S = 1/2$  spin operator at site  $i$ ; the first sum runs on nearest-neighbor bonds along the chains; and the second on bonds connecting nearest-neighboring chains to form a tetragonal lattice.  $\text{KCuF}_3$  has weak inter-chain coupling  $J_\perp = -1.6$  meV compared to the in-chain one  $J = 34$  meV [37], causing weak long-range Néel order to appear at a low critical temperature  $T_N = 39$  K  $\approx 0.1J$ . Nevertheless, many salient features of the one-dimensional physics (such as fractional excitations at sufficiently high energy [26] and entanglement properties [64]) are preserved to low  $T$  in spite of the long-range ordering.

In magnetic scattering such as from  $\text{KCuF}_3$  the local operators  $O_i$  are given by the spin components  $S_i^\mu$  with  $\mu = x, y, z$ , and the measured two-site dynamical structure factor is  $\chi''_{ij}(\mathbf{q}, \omega) = \sum_{\nu, \mu=x,y,z} (\delta_{\nu\mu} - \hat{q}_\nu \hat{q}_\mu) \chi''_{S_i^\nu, S_j^\mu}(\mathbf{q}, \omega)$  [38] where  $\hat{q}_\mu$  are the  $\mu = x, y, z$  components of the normalized scattering vector. In the Heisenberg (isotropic) limit, the spin components act identically and  $\chi''_{ij}(\omega) = \frac{1}{3} \sum_{\mu=x,y,z} \chi''_{S_i^\mu, S_j^\mu}(\omega)$ . The quantum correlation functions defined above can then be reconstructed, along with the total correlation function

$$C_{\text{tot}}(i, j) = \frac{1}{3} \langle \mathbf{S}_i \cdot \mathbf{S}_j \rangle = \frac{1}{\pi} \int d(\hbar\omega) \coth(\beta\hbar\omega/2) \chi''_{ij}(\omega). \quad (3)$$

The latter quantity is expected to exhibit an exponentially decaying behavior for  $T > T_N$ ,  $C_{\text{tot}}(i, j) \sim \exp(-|i - j|/\xi)$

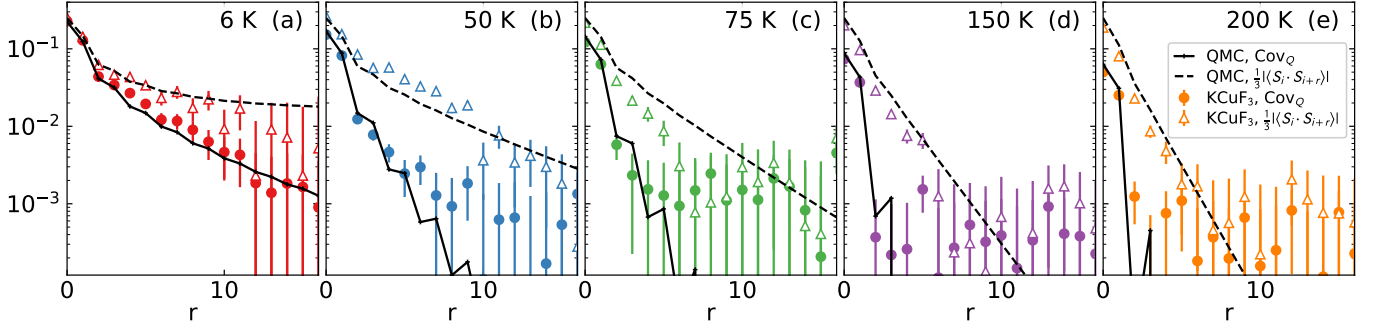


FIG. 2. **Total vs. quantum correlations in  $\text{KCuF}_3$ .** Reconstructed total and quantum correlations (expressed by the quantum covariance  $\text{Cov}_Q$ ) along the spin chains of  $\text{KCuF}_3$  at various temperatures, compared with numerically exact QMC data. The error bars represent one standard deviation uncertainty.

with  $\xi$  the correlation length; while the divergence of  $\xi$  at  $T_N$  entails the appearance of long-ranged correlations. On the other hand, the quantum covariance  $\text{Cov}_Q$  is expected to exhibit an exponential decay at *any* finite temperature,  $\text{Cov}_Q(i, j) \sim \exp(-|i - j|/\xi_Q)$  with  $\xi_Q$  defining the quantum coherence length, which is finite at any finite temperature, and coincides with  $\xi$  only for  $T \rightarrow 0$ . This behavior for  $\text{Cov}_Q$  has been numerically observed via QMC in Refs. [17, 23], and only recently it has been shown as a rigorous result [27]. Yet an experimental measurement of  $\xi_Q$  is still lacking to date.

*Quantum correlations for  $\text{KCuF}_3$ .*—Fig. 2 compares  $C_{\text{tot}}(i, j)$  and  $\text{Cov}_Q$  for sites  $i, j$  belonging to the same chain, as reconstructed from the neutron scattering structure factor of  $\text{KCuF}_3$  at various temperatures ( $T = 6, 50, 75, 150$  and  $200$  K) above and below  $T_N$ . The experimental data are compared with QMC data (obtained via the stochastic series expansion method [39]) for a  $10 \times 10$  array of 100-site spin chains. The experimental results beautifully match the theoretical ones, including the detailed structure clearly visible at short ranges. The vast difference between the correlation length and the emergent quantum coherence length is apparent: while the total correlations go from exponentially decaying (above  $T_N$ ) to decaying to a finite value (below  $T_N$ ), the quantum covariance clearly remains short-ranged at all temperatures, with a decay length  $\xi_Q$  which is significantly smaller than  $\xi$ . This implies that quantum correlations do not participate in the Néel transition, which is not surprising because of the classical nature of the finite-temperature phase transition.

The asymptotic exponential decay is clearly exhibited by  $C_{\text{tot}}(i, j)$  for  $T > T_N$  and distances exceeding a few lattice steps. The spatial structure of the quantum covariance is generally more complex (see Supplementary Material - SM - for an extended discussion [40]); yet a first exponential decay sets in after a few lattice steps, and this decay is clearly visible in the experimental data. We shall focus on the length associated with this short-range decay in the following, and extract it via a linear-regression (LR) estimator  $\xi_{Q,\text{LR}}$  from a linear fit of the logarithm of the correlation function ( $\xi_{Q,\text{LR}}$ ); or via a second-moment estimator  $\xi_{Q,2}$  (see Methods section). Fig. 3 shows the LR estimators for  $\xi$  and  $\xi_Q$ , comparing experiment

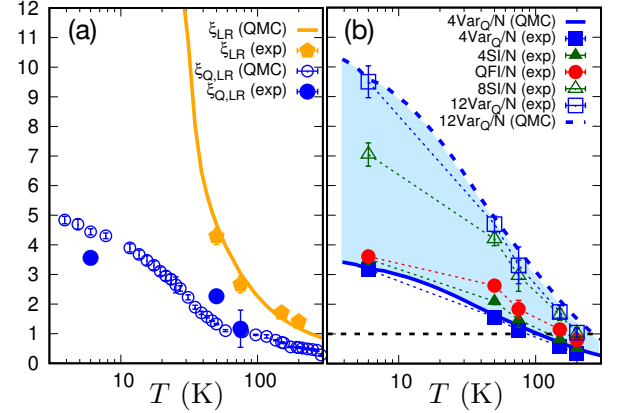


FIG. 3. **Quantum coherence length vs. entanglement depth.** (a) Quantum coherence length  $\xi_Q$  vs. total correlation length  $\xi$  as a function of temperature; (b) Entanglement depth estimated via the quantum fluctuations of the in-chain staggered magnetization, namely  $4\text{Var}_Q(M_{s,\text{chain}})/N$  and  $\text{QFI}(M_{s,\text{chain}})/N$ . The plot also shows  $12\text{Var}_Q/N$ , which is an upper bound to  $\text{QFI}(M_{s,\text{chain}})/N$ , as well as the lower and upper bounds on  $\text{QFI}(M_{s,\text{chain}})/N$  from the skew information,  $4\text{SI}/N$  and  $8\text{SI}/N$ . Both panels compare QMC data and experimental data on  $\text{KCuF}_3$ . The error bars represent one standard deviation uncertainty.

and numerical simulations, and exposing the large difference between the two length scales.

One may wonder how the spatial extension of quantum correlations relates to multipartite entanglement, namely the entanglement depth. In fact there is a rigorous relationship: the entanglement depth along the chains is bounded from below by the  $\text{Var}_Q$  density or the  $\text{QFI}$  density for the staggered magnetization  $M_s = \sum_r (-1)^r S_i^z$  of the individual chains, namely  $\text{Var}_Q(M_{s,\text{chain}})/N = \sum_r (-1)^r \text{Cov}_Q(i, i+r)$  and  $\text{QFI}(M_{s,\text{chain}})/N = \sum_r (-1)^r \text{QFIM}(i, i+r)$ , where  $r$  runs over distances along the chains. Indeed, when  $4\text{Var}_Q/N > k$  or when  $\text{QFI}/N > k$ , one can conclude that spins in each chain exhibit at least  $(k+1)$ -partite entanglement [16, 41, 42]. Fig. 3(b) shows the temperature dependence of  $4\text{Var}_Q$  and  $\text{QFI}$  for  $\text{KCuF}_3$ , compared with the theoretical results for

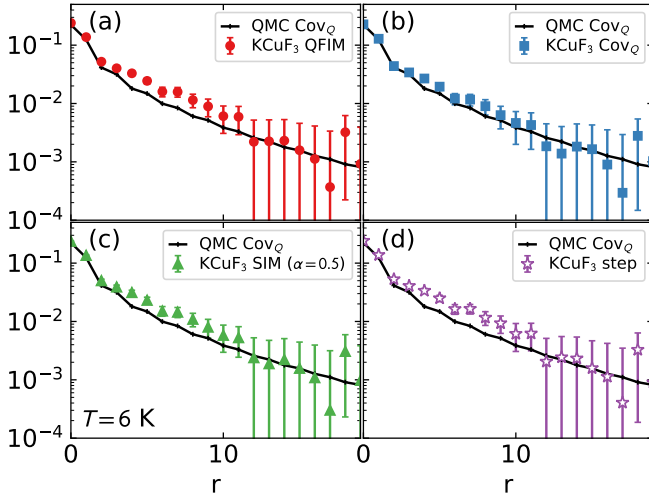


FIG. 4. **Various quantum correlation functions evaluated for  $\text{KCuF}_3$  at 6 K.** (a) The quantum Fisher information matrix, scaled as  $\text{QFIM}/4$ . (b) The quantum covariance  $\text{Cov}_Q$ . (c) The skew information matrix  $\text{SIM}$ . (d) Correlation function using the simple filter  $h^{\text{step}}(x)$  (see main text). In all panels the experimental data are compared with the QMC data for  $\text{Cov}_Q$  for reference. The error bars represent one standard deviation uncertainty.

$4\text{Var}_Q$ . Interestingly, the entanglement depth estimate offered by these quantities is comparable to the quantum coherence length, rising up to  $k + 1 = 4$ . In general one should expect quantum correlations to be systematically longer-ranged than the depth of entanglement, given that entanglement is a stronger form of correlation, and a quantum state can be quantum correlated without being entangled [11].

The various quantum correlation functions offered by Eq. (1) raise the question whether the quantum coherence length is uniquely defined, or whether it depends on the specific choice of quantum filter  $h$ . Fig. S1 shows that the same exponential decay is exhibited by all quantum correlation functions listed above ( $\text{Cov}_Q$ ,  $\text{QFIM}$ ,  $\text{SIM}$ ). In fact, it is a rather robust feature, uniquely stemming from the high-pass nature of  $h(x)$ . To emphasize the universality, we also calculate the most naive correlation using a step function filter,

$$h^{\text{step}}(x) = \begin{cases} 1 & \text{if } x/2 \geq 1 \\ 0 & \text{if } x/2 < 1 \end{cases} \quad (4)$$

such that all intensity below  $\hbar\omega/2k_B T$  is suppressed. Although this filter function lacks the linear behavior at small  $x$  required to define a proper quantum-coherence measure, it resembles more closely filter functions that are naturally applied in neutron-scattering experiments (see discussion below). The plot in Fig. S1(d) shows the same general behavior as the other quantum correlators. Thus, although details of the quantum correlators depend on the filter function, the revealed length scale appears universal.

**Redistribution of quantum correlations upon changing the interchain couplings.**— We now embed the quantum correlations in  $\text{KCuF}_3$  within the broader family of coupled spin

chain models described by the Hamiltonian Eq. (2). Using QMC simulations, we map the evolution of correlations and of quantum coherence along the chains upon varying the interchain coupling  $J_\perp$ , in order to explore the effect of the dimensionality of interactions. In the case of total correlations, an increase of  $|J_\perp|$  at fixed temperature drives the system from quasi-one-dimensional magnetism towards three-dimensional magnetism, *i.e.* towards a regime exhibiting stronger correlations in *all* spatial directions, both transverse and longitudinal to the chains. This behavior is clearly exhibited by the in-chain correlation length  $\xi_2$  shown in Fig. 5(a), whose sharp rise upon lowering the temperature marks the evolution of the Néel transition with the interchain coupling [43].

On the other hand, quantum correlations are found to undergo a rather different fate along the dimensional crossover of the couplings. Fig. 5(b-c) shows the  $T$  and  $J_\perp$  dependence of  $\xi_{Q,2}$  and  $\text{Var}_Q(M_{s,\text{chain}})/N$  (a lower bound to the in-chain entanglement depth). Contrary to total correlations, quantum correlations along the chains appear to *decrease* upon increasing the interchain couplings at low  $T$  (and the Néel transition is nearly invisible to  $\text{Var}_Q(M_{s,\text{chain}})/N$ ). The quantum coherence length  $\xi_Q$  is in fact found to increase again at sufficiently low temperature and sufficiently strong  $J_\perp$ , but this is an effect driven by the appearance of thin tails in the quantum correlation function which have little effect on the integral given by the quantum variance [40].

This result suggests that low-temperature quantum correlations in coupled-chain systems exhibit a form of *monogamy*, since a dimensional crossover in the couplings entails their spatial redistribution from in-chain to inter-chain correlations. In general, quantum correlations are not monogamous, as they are associated with multipartite entanglement, which can imply an arbitrary number of degrees of freedom. The above behavior suggests that the Heisenberg two-spin couplings are primarily promoting quantum correlations in the form of two-spin entanglement — presumably via singlet/triplet formation for antiferromagnetic/ferromagnetic couplings, respectively — which is indeed monogamous [44, 45]. As a result, quantum correlations along the chains decrease over shorter length scales when the interchain coupling is increased. This result shows that, among the family of coupled-chain Heisenberg models, quasi-one-dimensional compounds such as  $\text{KCuF}_3$  exhibit the strongest quantum correlations at short distance, whose detection via neutron scattering is most efficient. (In the Supplemental Information [40] we also show that inter-chain quantum correlations do not rise to the same strength as that of intrachain ones over the range of interchain couplings explored in this study.)

**Discussion.** These results have exciting implications far beyond 1D spin chains. Firstly, our results on 1D chains demonstrate that the spatial structure of quantum correlations reveals new *quantitative* information about the dimensionality of quantum materials, a fundamental property inherently linked to quantum statistics and novel phases of matter. This is important as “low-dimensional materials” often exist in a three-dimensional host crystal and retain weak three-



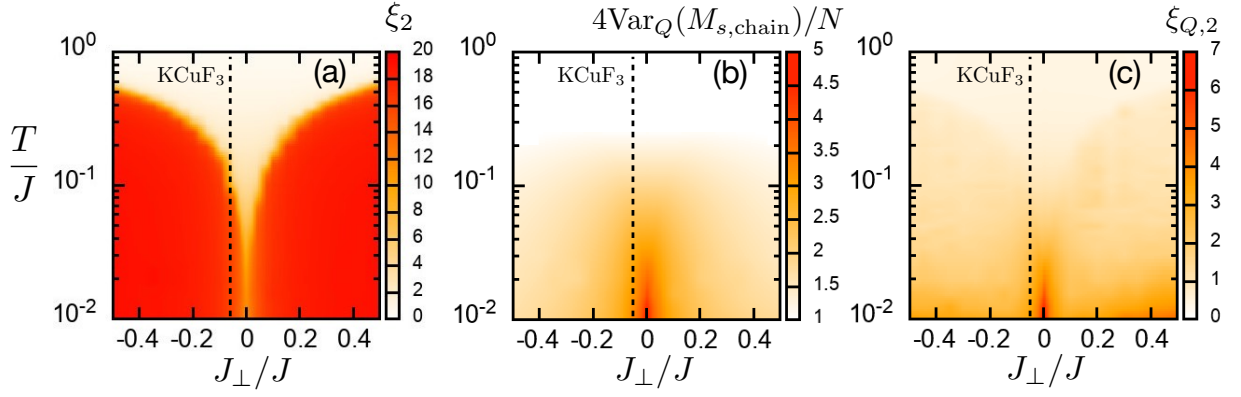


FIG. 5. **Total vs. quantum correlations for coupled Heisenberg chains from QMC data.** (a) Second-moment estimator for the in-chain correlation length  $\xi_2$ , showing clearly the Néel order; (b) Quantum variance per spin of the in-chain staggered magnetization,  $4\text{Var}_Q(M_{s,\text{chain}})/N$ ; (c) second-moment estimator for the in-chain quantum coherence length  $\xi_{Q,2}$ . In all panels, the dashed line marks the value of  $J_{\perp}/J$  realized by  $\text{KCuF}_3$ .

dimensional coupling. Our methods give access to the effective dimensionalities of quantum and total correlations, which may be rather different in general, as our results clearly show. In this respect, it is important to note that our quantum correlator analysis is not restricted to neutron spectroscopy: any momentum-resolved probe of dynamic susceptibility associated with local Hermitian operators will work in the same fashion. For instance, quantum correlations in the charge sector could be probed via X-ray scattering [46] or electron energy-loss spectroscopy [47], offering complementary pictures of quantum coherence in a huge variety of quantum materials.

Secondly, the quantum correlators are model-independent, which allows precise statements to be made about materials even in the absence of tractable theory. Therefore they may yield important information about enigmatic condensed matter states. For example, one could evaluate how the spatial structure of quantum correlations changes across quantum phase transitions (as in, e.g., heavy fermion materials [48] or quantum magnets under fields). Recent works [17, 49] showed that quantum correlations can reconstruct the quantum critical fan occurring at finite temperatures above such quantum critical points, thus certifying quantum criticality and delineating the range of genuine quantum critical behavior. Within the space of coupled spin chains, it would be interesting to apply the same analysis to systems with frustrated interchain coupling, such as  $\text{Cs}_2\text{CuCl}_4$  [50, 51], in order to test if frustration can stabilize the intrachain quantum correlation length compared to the unfrustrated case studied here.

Thirdly and more generally, our results advance the synthesis of condensed matter physics and quantum information. Specifically, we show that experimental momentum-resolved dynamical response functions at thermal equilibrium can be mined for a wealth of many-body quantum information. The ability to do this for a thermodynamic system at a well-defined temperature is not shared by many other platforms for quantum many-body physics. (For example, most quantum many-

body physics simulators based on atomic physics platforms do not operate at thermal equilibrium; or, if they do so, their temperature is not easily accessible or cannot easily be held fixed [52–54]. As a consequence, a similar analysis to ours cannot be straightforwardly conducted with e.g. cold atoms.) Hence our results indicate a clear path for experiments on quantum materials to positively contribute to quantum information theory, by revealing the microscopic structure of quantum correlations in many-body states.

On a different note, the fact that the step function filter captures the same behavior as the other quantum correlators suggests that approximate results for the quantum length scale can be experimentally obtained by neutron diffraction methods. At low temperatures where  $\chi''(\mathbf{k}, \omega) \approx \pi S(\mathbf{k}, \omega)$ , the filter function  $h^{\text{step}}(x)$  can be traded for a physical neutron transmission filter (e.g., beryllium powder) [55, 56], tuning the incident neutron energy to act as a high-pass filter. For suitable systems (specifically, low-bandwidth materials such as  $\text{CuSO}_4 \cdot 5\text{D}_2\text{O}$  [57],  $\text{YbAlO}_3$  [58], and  $\text{Cs}_2\text{CoCl}_4$  [20]) it offers a path towards quickly identifying if a material has significant quantum correlations.

**Conclusions.** We have shown how the spatial structure of quantum correlation functions for quantum spin systems can be extracted from neutron spectroscopy data. The data reveal the existence of a fundamental length scale of quantum mechanical origin — the quantum coherence length — limiting the range of quantum correlations at all finite temperatures, which is wildly different from the correlation length. Our study also highlights the role of dimensionality on quantum correlations, showing that a stronger coupling between Heisenberg chains leads to a redistribution of quantum correlations from the chains to the transverse directions, in contrast to total correlations. As a consequence, within the family of coupled-chain compounds, systems close to the one-dimensional limit — such as  $\text{KCuF}_3$  — exhibit the strongest short-range quantum correlations and the weakest total correlations. The fact that quantum correlators enabled new

observations—even for a well-studied model as the one-dimensional Heisenberg chain—indicates that quantum correlator analysis could be a powerful new way of assessing the underlying quantum state of a vast number of quantum materials, both low- and higher-dimensional.

## ACKNOWLEDGEMENTS

We thank I. Frérot for valuable discussions. The work by A.S. and D.A.T. is supported by the Quantum Science Center (QSC), a National Quantum Information Science Research Center of the U.S. Department of Energy (DOE). The work of P.L. and E.D. was supported by the U.S. Department of Energy, Office of Science, Basic Energy Sciences, Materials Sciences and Engineering Division. All QMC calculations have been performed on the PSMN cluster at the ENS of Lyon.

## AUTHOR CONTRIBUTIONS

A.S., P.L., and T.R. conceived and coordinated the project. A.S. analyzed the neutron data. QMC calculations were performed by T.R., and DMRG calculations by P.L. The manuscript was written by A.S., P.L., and T.R. with input from all co-authors.

## Methods

### Definitions of the quantum correlation functions and quantum coherence measures.

The measurement of the momentum-resolved dynamical susceptibility via neutron scattering allows one to reconstruct any quantum correlation function  $C[O_i, O_j; h, \rho]$  for the state  $\rho$  having the form of Eq. (1) of the main text, dependent on the filter function  $h$ . The double sum of the quantum correlation function over its indices reconstructs in turn a relevant quantum coherence measure,  $I[O; h, \rho] = \sum_{ij} C[O_i, O_j; h, \rho]$ . In our work we explored the following coherence measures, and related quantum correlation functions (we cite again the quantum covariance for completeness):

1. the quantum Fisher information (QFI),  $I[O; 4h_{\text{QFI}}, \rho] = \text{QFI}(O; \rho)$  for which [15, 31, 59]

$$h_{\text{QFI}}(x) = \tanh(x/2).$$

$C[O_i, O_j; 4h_{\text{QFI}}, \rho] = \text{QFIM}[O_i, O_j; \rho]$  expresses the quantum Fisher information matrix (QFIM) [33];

2. the quantum variance ( $\text{Var}_Q$ ) [16]  $I[O; h_{\text{Var}_Q}, \rho] = \text{Var}_Q(O; \rho)$  for which

$$h_{\text{Var}_Q}(x) = \mathcal{L}(x/2),$$

where  $\mathcal{L}(x) = \coth x - 1/x$  the Langevin function.  $C[O_i, O_j; h_{\text{Var}_Q}, \rho] = \text{Cov}_Q[O_i, O_j; \rho]$  expresses the quantum covariance ( $\text{Cov}_Q$ ) [17, 23]; and

3. the Wigner-Yanase-Dyson skew information (SI) [24]  $I[O; h_\alpha, \rho] = \text{SI}_\alpha(O; \rho)$ , for which

$$h_\alpha(x) = \frac{\cosh(x/2) - \cosh[(\alpha - 1/2)x]}{\sinh(x/2)},$$

where  $0 < \alpha < 1$  is a parameter that takes the value of  $\alpha = 1/2$  in the original Wigner-Yanase definition [24], with  $h_{1/2} = \tanh(x/4)$ .  $C[O_i, O_j; h_\alpha, \rho] = \text{SIM}_\alpha[O_i, O_j; \rho]$  expresses the skew-information matrix (SIM).

The  $\text{Var}_Q$  and  $\text{Cov}_Q$  can be in fact obtained as the average of  $\text{SI}_\alpha$  and  $\text{SIM}_\alpha$  (respectively) on the  $\alpha$  index, since  $\int_0^1 d\alpha h_\alpha(x) = \mathcal{L}(x/2)$ . SI and SIM without the argument  $\alpha$  refer implicitly to the case  $\alpha = 1/2$ , which is the one we focused on with the results shown in the main text. All the above quantities are intimately linked by the inequality chain  $\text{Var}_Q[O; \rho] \leq \text{SI}[O; \rho] \leq \text{QFI}[O; \rho]/4 \leq 2\text{SI}[O; \rho] \leq 3\text{Var}_Q[O; \rho]$ .

The SI and SIM can be expressed in terms imaginary-time correlation functions [31], and therefore, similarly to  $\text{Var}_Q$  and  $\text{Cov}_Q$ , they are accessible to QMC. On the other hand, the QFI and QFIM requires instead the full reconstruction of the dynamical susceptibility, which is not accessible to QMC directly, due to a notoriously ill-defined analytical continuation of time-dependent correlations from imaginary to real time [60].

### Second-moment estimators

Figs. 5(a) and 5(c) show the second-moment estimator for the in-chain correlation length and quantum coherence length respectively, defined as

$$\xi_2^2 = \frac{1}{2} \frac{\sum_r r^2 |\langle \mathbf{S}_i \cdot \mathbf{S}_{i+r} \rangle|}{\sum_r |\langle \mathbf{S}_i \cdot \mathbf{S}_{i+r} \rangle|} \quad (5)$$

for the correlation length; and similarly for the quantum coherence length, obtained by substituting  $|\langle \mathbf{S}_i \cdot \mathbf{S}_{i+r} \rangle|$  with  $\text{Cov}_Q(i, i+r)$ . These estimators allow for a systematic extraction of a typical length from all the correlation data produced with QMC across the vast parameter range explored in Fig. 5. In the case of the quantum correlations, Fig. 5(c) shows that this estimator for the quantum coherence length is sensitive to the buildup of a thin tail for large  $|J_\perp|$ , as shown by the seemingly non-monotonic behavior of  $\xi_{Q,2}$  when increasing  $|J_\perp|$ . Indeed at very low  $T$ ,  $\xi_{Q,2}$  is first decreasing for small  $|J_\perp|$ , and then it increases again for larger  $|J_\perp|$ . See the Supplemental Material for more details on the tails in  $\text{Cov}_Q$  [40].

## Experimental data processing

All experimental data used in this study was previously published in [35], which involved a composite data set from two different neutron experiments for temperatures  $T = 75$  K and above: SEQUOIA at the SNS [61] for low energy, and MAPS at ISIS [62] for high energy. The data at  $T = 6$  K and 50 K are from ISIS. For the quantum correlators, we applied the formulae to the data as previously processed. However, for the conventional correlation length at  $T = 6$  K, we applied a resolution deconvolution. This is because  $\text{KCuF}_3$  at  $T = 6$  K has long range magnetic order and a very long correlation length ( $\sim 700$  sites [63]). Consequently, resolution broadening has to be corrected before the true long range correlations will emerge. We did this by fitting the  $q = \pi$   $T = 6$  K  $\hbar\omega = 0$  scattering to a Gaussian function, and dividing the Fourier transformed structure factor by the Fourier transformed Gaussian function. This resulted in a visible increase in total correlations for  $r > 15$ . For only the  $T = 6$  K conventional correlations did this correction make any visible difference.

- 
- [1] R. Horodecki, P. Horodecki, M. Horodecki, and K. Horodecki, Rev. Mod. Phys. **81**, 865 (2009), URL <https://link.aps.org/doi/10.1103/RevModPhys.81.865>.
  - [2] N. Brunner, D. Cavalcanti, S. Pironio, V. Scarani, and S. Wehner, Rev. Mod. Phys. **86**, 419 (2014), URL <https://link.aps.org/doi/10.1103/RevModPhys.86.419>.
  - [3] X.-L. Wang, L.-K. Chen, W. Li, H.-L. Huang, C. Liu, C. Chen, Y.-H. Luo, Z.-E. Su, D. Wu, Z.-D. Li, et al., Phys. Rev. Lett. **117**, 210502 (2016), URL <https://link.aps.org/doi/10.1103/PhysRevLett.117.210502>.
  - [4] P. Thomas, L. Ruscio, O. Morin, and G. Rempe, Nature **608**, 677–681 (2022), ISSN 1476-4687, URL <https://doi.org/10.1038/s41586-022-04987-5>.
  - [5] T. Monz, P. Schindler, J. T. Barreiro, M. Chwalla, D. Nigg, W. A. Coish, M. Harlander, W. Hänsel, M. Hennrich, and R. Blatt, Phys. Rev. Lett. **106**, 130506 (2011), URL <https://link.aps.org/doi/10.1103/PhysRevLett.106.130506>.
  - [6] R. Schmied, J.-D. Bancal, B. Allard, M. Fadel, V. Scarani, P. Treutlein, and N. Sangouard, Science **352**, 441–444 (2016), URL <https://science.sciencemag.org/content/352/6284/441>.
  - [7] A. Omran, H. Levine, A. Keesling, G. Semeghini, T. T. Wang, S. Ebadi, H. Bernien, A. S. Zibrov, H. Pichler, S. Choi, et al., Science **365**, 570–574 (2019), URL <https://www.science.org/doi/abs/10.1126/science.aax9743>.
  - [8] C. Song, K. Xu, H. Li, Y.-R. Zhang, X. Zhang, W. Liu, Q. Guo, Z. Wang, W. Ren, J. Hao, et al., Science **365**, 574–577 (2019), URL <https://www.science.org/doi/abs/10.1126/science.aay0600>.
  - [9] G. J. Mooney, C. D. Hill, and L. C. L. Hollenberg, Sci. Rep. **9**, 13465 (2019), ISSN 2045-2322, URL <https://doi.org/10.1038/s41598-019-49805-7>.
  - [10] B. Keimer and J. Moore, Nat. Phys. **13**, 1045–1055 (2017), URL <https://doi.org/10.1038/nphys4302>.
  - [11] G. Adesso, T. R. Bromley, and M. Cianciaruso, J. Phys. A: Math. Theor. **49**, 473001 (2016), URL <https://dx.doi.org/10.1088/1751-8113/49/47/473001>.
  - [12] G. D. Chiara and A. Sanpera, Rep. Prog. Phys. **81**, 074002 (2018), URL <https://dx.doi.org/10.1088/1361-6633/aabf61>.
  - [13] L. Pezzè, A. Smerzi, M. K. Oberthaler, R. Schmied, and P. Treutlein, Rev. Mod. Phys. **90**, 035005 (2018), URL <https://link.aps.org/doi/10.1103/RevModPhys.90.035005>.
  - [14] I. Frérot, M. Fadel, and M. Lewenstein, *Probing quantum correlations in many-body systems: a review of scalable methods* (2023), 2302.00640, URL <https://arxiv.org/abs/2302.00640>.
  - [15] P. Hauke, M. Heyl, L. Tagliacozzo, and P. Zoller, Nat. Phys. **12**, 778–782 (2016), URL <https://doi.org/10.1038/nphys3700>.
  - [16] I. Frérot and T. Roscilde, Phys. Rev. B **94**, 075121 (2016), URL <https://link.aps.org/doi/10.1103/PhysRevB.94.075121>.
  - [17] I. Frérot and T. Roscilde, Nat. Commun. **10**, 577 (2019), URL <https://doi.org/10.1038/s41467-019-08324-9>.
  - [18] G. Mathew, S. L. L. Silva, A. Jain, A. Mohan, D. T. Adroja, V. G. Sakai, C. V. Tomy, A. Banerjee, R. Goreti, A. V.N., et al., Phys. Rev. Research **2**, 043329 (2020), URL <https://link.aps.org/doi/10.1103/PhysRevResearch.2.043329>.
  - [64] A. Scheie, P. Laurell, A. M. Samarakoon, B. Lake, S. E. Nagler, G. E. Granroth, S. Okamoto, G. Alvarez, and D. A. Tennant, Phys. Rev. B **103**, 224434 (2021), URL <https://link.aps.org/doi/10.1103/PhysRevB.103.224434>.
  - [20] P. Laurell, A. Scheie, C. J. Mukherjee, M. M. Koza, M. Enderle, Z. Tylczynski, S. Okamoto, R. Coldea, D. A. Tennant, and G. Alvarez, Phys. Rev. Lett. **127**, 037201 (2021), URL <https://link.aps.org/doi/10.1103/PhysRevLett.127.037201>.
  - [21] S. L. Braunstein and C. M. Caves, Phys. Rev. Lett. **72**, 3439 (1994), URL <https://link.aps.org/doi/10.1103/PhysRevLett.72.3439>.
  - [22] A. O. Scheie, E. A. Ghioldi, J. Xing, J. A. M. Paddison, N. E. Sherman, M. Dupont, D. Abernathy, D. M. Pajerowski, S.-S. Zhang, L. O. Manuel, et al. (2021), arXiv:2109.11527, URL <https://arxiv.org/abs/2109.11527>.
  - [23] D. Malpetti and T. Roscilde, Phys. Rev. Lett. **117**, 130401 (2016), URL <https://link.aps.org/doi/10.1103/PhysRevLett.117.130401>.
  - [24] E. P. Wigner and M. M. Yanase, Proc. Natl. Acad. Sci. U.S.A. **49**, 910–918 (1963), URL <https://doi.org/10.1073/pnas.49.6.910>.
  - [25] B. Lake, D. A. Tennant, C. D. Frost, and S. E. Nagler, Nat. Mater. **4**, 329–334 (2005), URL <https://doi.org/10.1038/nmat1327>.
  - [26] B. Lake, D. A. Tennant, J.-S. Caux, T. Barthel, U. Schollwöck, S. E. Nagler, and C. D. Frost, Phys. Rev. Lett. **111**, 137205 (2013), URL <https://link.aps.org/doi/10.1103/PhysRevLett.111.137205>.
  - [27] T. Kuwahara and K. Saito, Phys. Rev. X **12**, 021022 (2022), URL <https://link.aps.org/doi/10.1103/PhysRevX.12.021022>.
  - [28] D. Forster, *Hydrodynamic Fluctuations, Broken Symmetry, and Correlation Functions*, Advanced book classics (Avalon Publishing, 1995), ISBN 9780201410495.
  - [29] D. Petz, Linear Algebra Appl. **244**, 81–96 (1996), ISSN 0024-3795, URL <http://www.sciencedirect.com/science/article/pii/S0024379594002118>.

- [30] P. Gibilisco, D. Imparato, and T. Isola, *Proc. Amer. Math. Soc.* **137**, 317–327 (2009), URL <https://doi.org/10.1090/S0002-9939-08-09447-1>.
- [31] I. Frérot, Ph.D. thesis, École normale supérieure de Lyon (2017), URL <https://tel.archives-ouvertes.fr/tel-01679743>.
- [32] I. Frérot, A. Rançon, and T. Roscilde, *Phys. Rev. Lett.* **128**, 130601 (2022), URL <https://link.aps.org/doi/10.1103/PhysRevLett.128.130601>.
- [33] J. Liu, H. Yuan, X.-M. Lu, and X. Wang, *J. Phys. A: Math. Theor.* **53**, 023001 (2019), URL <https://dx.doi.org/10.1088/1751-8121/ab5d4d>.
- [34] S. Lovesey, *Theory of Neutron Scattering from Condensed Matter* (Clarendon Press, Oxford, 1984).
- [35] A. Scheie, P. Laurell, B. Lake, S. E. Nagler, M. B. Stone, J.-S. Caux, and D. A. Tennant, *Nat. Commun.* **13**, 5796 (2022), URL <https://doi.org/10.1038/s41467-022-33571-8>.
- [36] D. A. Tennant, T. G. Perring, R. A. Cowley, and S. E. Nagler, *Phys. Rev. Lett.* **70**, 4003 (1993), URL <https://link.aps.org/doi/10.1103/PhysRevLett.70.4003>.
- [37] B. Lake, D. A. Tennant, and S. E. Nagler, *Phys. Rev. B* **71**, 134412 (2005), URL <https://link.aps.org/doi/10.1103/PhysRevB.71.134412>.
- [38] G. L. Squires, *Introduction to the Theory of Thermal Neutron Scattering* (Cambridge University Press, Cambridge, UK, 2012), 3rd ed.
- [39] O. F. Syljuåsen and A. W. Sandvik, *Phys. Rev. E* **66**, 046701 (2002), URL <https://link.aps.org/doi/10.1103/PhysRevE.66.046701>.
- [40] See Supplemental Material (SM) for further numerical data and details about the spatial structure of the quantum covariance, and its reconfiguration upon increasing the interchain couplings.
- [41] P. Hyllus, W. Laskowski, R. Krischek, C. Schwemmer, W. Wiczorek, H. Weinfurter, L. Pezzé, and A. Smerzi, *Phys. Rev. A* **85**, 022321 (2012), URL <https://link.aps.org/doi/10.1103/PhysRevA.85.022321>.
- [42] G. Tóth, *Phys. Rev. A* **85**, 022322 (2012), URL <https://link.aps.org/doi/10.1103/PhysRevA.85.022322>.
- [43] C. Yasuda, S. Todo, K. Hukushima, F. Alet, M. Keller, M. Troyer, and H. Takayama, *Phys. Rev. Lett.* **94**, 217201 (2005), URL <https://link.aps.org/doi/10.1103/PhysRevLett.94.217201>.
- [44] V. Coffman, J. Kundu, and W. K. Wootters, *Phys. Rev. A* **61**, 052306 (2000), URL <https://link.aps.org/doi/10.1103/PhysRevA.61.052306>.
- [45] T. J. Osborne and F. Verstraete, *Phys. Rev. Lett.* **96**, 220503 (2006), URL <https://link.aps.org/doi/10.1103/PhysRevLett.96.220503>.
- [46] W. Schülke, *Electron Dynamics by Inelastic X-ray Scattering*, vol. 7 of *Oxford Series on Synchrotron Radiation* (Oxford University Press, 2007).
- [47] S. Vig, A. Kogar, M. Mitrano, A. A. Husain, V. Mishra, M. S. Rak, L. Venema, P. D. Johnson, G. D. Gu, E. Fradkin, et al., *SciPost Phys.* **3**, 026 (2017), URL <https://scipost.org/10.21468/SciPostPhys.3.4.026>.
- [48] P. Gegenwart, Q. Si, and F. Steglich, *Nat. Phys.* **4**, 186–197 (2008), URL <https://doi.org/10.1038/nphys892>.
- [49] M. Gabbriellini, A. Smerzi, and L. Pezzè, *Sci. Rep.* **8**, 15663 (2018), ISSN 2045-2322, URL <http://www.nature.com/articles/s41598-018-31761-3>.
- [50] R. Coldea, D. A. Tennant, K. Habicht, P. Smeibidl, C. Wolters, and Z. Tylczynski, *Phys. Rev. Lett.* **88**, 137203 (2002), URL <https://link.aps.org/doi/10.1103/PhysRevLett.88.137203>.
- [51] O. A. Starykh, H. Katsura, and L. Balents, *Phys. Rev. B* **82**, 014421 (2010), URL <https://link.aps.org/doi/10.1103/PhysRevB.82.014421>.
- [52] D. C. McKay and B. DeMarco, *Rep. Prog. Phys.* **74**, 054401 (2011), URL <https://dx.doi.org/10.1088/0034-4885/74/5/054401>.
- [53] S. Trotzky, L. Pollet, F. Gerbier, U. Schnorrberger, I. Bloch, N. V. Prokof'ev, B. Svistunov, and M. Troyer, *Nat. Phys.* **6**, 998–1004 (2010), ISSN 1745-2481, URL <https://doi.org/10.1038/nphys1799>.
- [54] C. Carcy, G. Hercé, A. Tenart, T. Roscilde, and D. Clément, *Phys. Rev. Lett.* **126**, 045301 (2021), URL <https://link.aps.org/doi/10.1103/PhysRevLett.126.045301>.
- [55] P. Egelstaff and R. Pease, *J. Sci. Instrum.* **31**, 207 (1954), URL <https://dx.doi.org/10.1088/0950-7671/31/6/305>.
- [56] D. Tennant, *Rev. Sci. Instrum.* **59**, 380–381 (1988), URL <https://doi.org/10.1063/1.1140212>.
- [57] M. Mourigal, M. Enderle, A. Klöpperpieper, J.-S. Caux, A. Stunault, and H. M. Rønnow, *Nat. Phys.* **9**, 435–441 (2013), URL <https://doi.org/10.1038/nphys2652>.
- [58] L. S. Wu, S. E. Nikitin, Z. Wang, W. Zhu, C. D. Batista, A. M. Tsvelik, A. M. Samarakoon, D. A. Tennant, M. Brando, L. Vasyilechko, et al., *Nat. Commun.* **10**, 698 (2019), URL <https://doi.org/10.1038/s41467-019-08485-7>.
- [59] I. Frérot, A. Rançon, and T. Roscilde, *Phys. Rev. Lett.* **128**, 130601 (2022), URL <https://link.aps.org/doi/10.1103/PhysRevLett.128.130601>.
- [60] M. Jarrell and J. Gubernatis, *Physics Reports* **269**, 133–195 (1996), ISSN 0370-1573, URL <https://www.sciencedirect.com/science/article/pii/0370157395000747>.
- [61] G. E. Granroth, A. I. Kolesnikov, T. E. Sherline, J. P. Clancy, K. A. Ross, J. P. C. Ruff, B. D. Gaulin, and S. E. Nagler, *J. Phys.: Conf. Ser.* **251**, 012058 (2010), URL <https://doi.org/10.1088/1742-6596/251/1/012058>.
- [62] T. Perring, A. Taylor, R. Osborn, D. Paul, A. Boothroyd, and G. Aeppli, *RAL Report* **94**, 1 (1994).
- [63] H. Ikeda and K. Hirakawa, *J. Phys. Soc. Jpn.* **35**, 722–728 (1973), URL <https://doi.org/10.1143/JPSJ.35.722>.



# Supplementary Information for Reconstructing the spatial structure of quantum correlations

Allen Scheie,<sup>1</sup> Pontus Laurell,<sup>2</sup> Elbio Dagotto,<sup>2,3</sup> D. Alan Tennant,<sup>2</sup> and Tommaso Roscilde<sup>4</sup>

<sup>1</sup>*MPA-Q, Los Alamos National Laboratory, Los Alamos, NM 87545, USA*

<sup>2</sup>*Department of Physics and Astronomy, University of Tennessee, Knoxville, Tennessee 37996, USA*

<sup>3</sup>*Materials Science and Technology Division, Oak Ridge National Laboratory, Oak Ridge, Tennessee 37831, USA*

<sup>4</sup>*Univ Lyon, ENS de Lyon, CNRS, Laboratoire de Physique, F-69342 Lyon, France*

(Dated: June 21, 2023)

## Comparing quantum correlators

For a comparison of the experimental and theoretical quantum correlators at all measured temperatures, see Fig. S1. Note that above  $T = 75$  K, only a few nearest neighbors have quantum correlations distinguishable from the large  $r$  background noise. This is a consequence of the experimental background in  $\text{KCuF}_3$ , which was previously discussed in Ref. [64].

The DMRG data for the QFIM on isolated chains at finite temperature, shown in Fig. S1, may erroneously suggest that the latter quantity possesses a decay length which is systematically larger than that of e.g.  $\text{Cov}_Q$ . This discrepancy is in fact not intrinsic, but it is rather the result of the fact that the DMRG calculations are done on isolated chains, while the theoretical curves for  $\text{Cov}_Q$  are QMC data for coupled chains. Indeed, as noted in the main text, the strength of the interchain coupling  $J_\perp$  makes a dramatic difference in the length scale of the quantum correlator. Figure S2 shows this more explicitly, with  $\text{Cov}_Q$  plotted for the  $\text{KCuF}_3$  value of  $J_\perp$  and for  $J_\perp = 0$ . See also the detailed discussion of this topic in the next section.

In the case of one-dimensional QMC simulations, we also show the comparison between the quantum covariances on two different system sizes ( $L = 100$  and  $L = 200$ ). The data display minor differences over the range of distances which are relevant for the experiment. We therefore conclude that the QMC data we use for the quantum covariance are essentially devoid of significant finite-size effects.

## Evolution of quantum correlations upon changing the interchain couplings

Here we discuss the detailed evolution of the spatial structure of quantum correlations upon changing the strength of the coupling between Heisenberg chains, as stemming from our experimental as well as theoretical data. Fig. S3 shows the comparison between the experimental data on two different quantum correlation functions (quantum covariance and the quantum Fisher information matrix) for  $\text{KCuF}_3$  at  $T = 6$  K, and theoretical data obtained for a single one-dimensional chain. In particular the theory data on quantum covariance are obtained via quantum Monte Carlo (QMC) as in the main text. On the other hand, the data for the quantum Fisher information matrix are inaccessible to QMC, because they require

the full knowledge of the dynamical susceptibility. For one-dimensional system, this knowledge can be obtained using the density-matrix renormalization group (DMRG) [65, 66], which allows for the calculation of  $S(k, \omega)$  at finite temperature [67, 68]. Here we extend the finite- $T$  calculations reported in Ref. [64] down to  $T = 6$  K. We use the DMRG++ software [69] to study a system with open boundary conditions, consisting of  $L = 50$  physical sites, and 50 “ancilla” sites.  $S(k, \omega)$  spectra are calculated using the Krylov-space correction vector method [70, 71], with a Lorentzian energy broadening with half width at half maximum  $\eta = 0.1J$ . For details on how to reproduce the DMRG calculations, see the supplemental material of Ref. [64].

As seen in Fig. S3, the predictions for the quantum correlation functions of a single one-dimensional chain lie systematically above the measured values for  $\text{KCuF}_3$ , while a much better quantitative agreement is obtained when taking into account the small albeit finite interchain coupling  $J_\perp$ , as shown in Fig. S3(b). This indicates that, 1) the resolution of the experiment is clearly sufficient to reconstruct the difference between isolated vs. weakly coupled Heisenberg chains, and 2) moving from a single chain to coupled chains, quantum correlations reorganize spatially, in such a way that correlations along the chains are suppressed.

We examine this trend systematically via QMC, by monitoring how the spatial structure of the quantum covariance changes upon increasing the magnitude of the ferromagnetic coupling ( $J_\perp < 0$ ) between the chains. In particular we examine the quantum covariance at  $T = 6$  K (assuming an in-chain coupling equal to that of  $\text{KCuF}_3$ ) along the chains, namely  $\text{Cov}_Q(i, i+x)$ , taking  $x$  as the direction of extension of the chains; and perpendicular to the chains, namely  $\text{Cov}_Q(i, i+y)$ , where  $y$  is one of the two perpendicular lattice directions. Fig. S4 shows that, upon increasing  $|J_\perp|$ , the correlations along a coordinate axis perpendicular to the chain become stronger, as can be trivially expected – albeit remaining much weaker than the in-chain correlations for the whole range of values of  $J_\perp$  we explored ( $|J_\perp| \leq J/2$ ). On the other hand, the in-chain quantum covariance undergoes a much more complex evolution: it becomes significantly weaker at short range when  $|J_\perp|$  increases, witnessing a form of monogamy of short-range quantum correlations, as discussed in the main text. Yet the behavior at long range shows an opposite trend for sufficiently large  $|J_\perp|$ , as the in-chain quantum covariance develops a stronger tail. This tail can be associated with the appearance of long-range *multipartite* quantum correlations. Such corre-

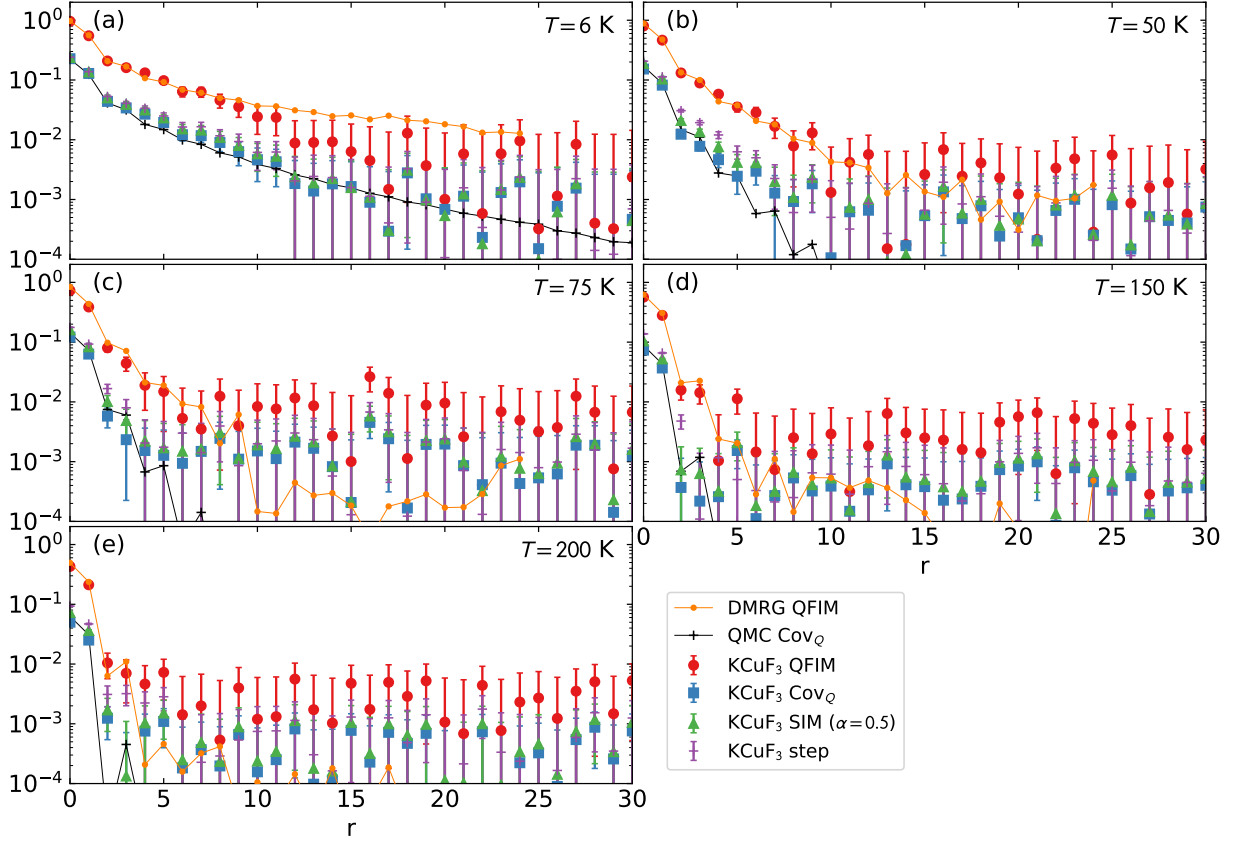


FIG. S1. **Full temperature dependence of the quantum correlation functions.** Absolute values of various definitions of quantum correlator applied to  $\text{KCuF}_3$  at temperatures between  $T = 6$  K and  $T = 200$  K, as well as QMC and DMRG calculations for comparison. Panel (a) corresponds to Fig. 4 in the main text, but with the raw values of QFI matrix.

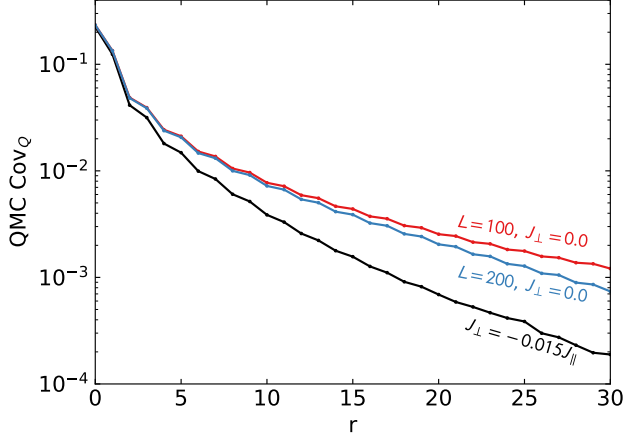


FIG. S2. **Quantum covariance from quantum Monte Carlo (QMC) for coupled and uncoupled chains.** The quantum covariance is much longer ranged in the one-dimensional  $J_\perp = 0$  limit. Meanwhile the chain length slightly decreases the length scale, in accord with the periodic boundary being further away.

mous. Nonetheless, the long-range tail is rather thin, and it gives a small contribution to the quantum variance of the in-chain staggered magnetization, so that the global trend is a decrease of this quantity with  $|J_\perp|$ , as shown in Fig. 5(b) of the main text.

The buildup of increasingly strong multipartite quantum correlations and entanglement upon coupling the chains is clearly exhibited in Fig. S5, in which the quantum variance density of the order parameter  $M_{\mathbf{Q}} = \sum_i e^{i\mathbf{Q}\cdot\mathbf{r}_i} S_i^z$  is shown; the ordering vector  $\mathbf{Q}$  being  $(\pi, 0, 0)$  for  $J_\perp < 0$  and  $(\pi, \pi, \pi)$  for  $J_\perp = 0$ . One clearly observes that rather massive entanglement sets in at low temperatures in the more strongly coupled chains – involving  $> 40$  spins within the temperature and parameter range we explored. Yet this behavior really stems from the buildup of correlations transverse to the chains – as can be easily deduced by comparing with Fig. 5(b) of the main text.

lations are expected in a long-range-ordered quantum ground state, such as that of a system of coupled Heisenberg chains; and their multipartite nature makes them no longer monoga-

[64] A. Scheie, P. Laurell, A. M. Samarakoon, B. Lake, S. E. Nagler, G. E. Granroth, S. Okamoto, G. Alvarez, and D. A. Tennant, Phys. Rev. B **103**, 224434 (2021), URL <https://link.aps.org/doi/10.1103/PhysRevB.103.224434>

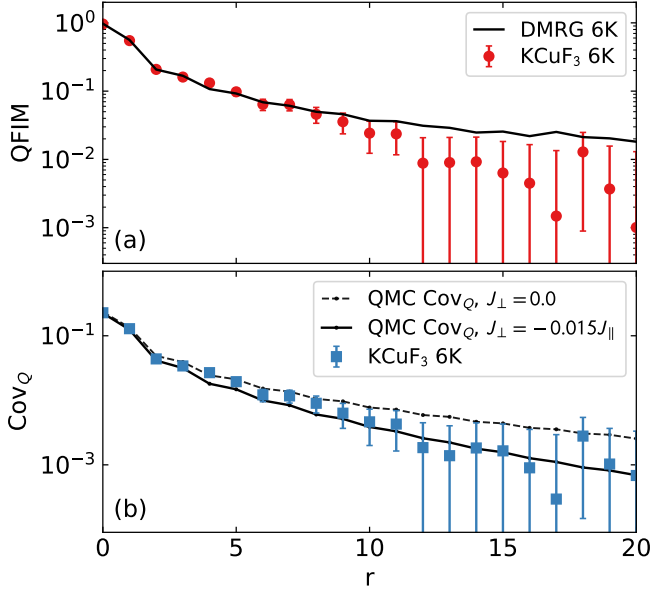


FIG. S3. Comparison between 1d theoretical QFIM (a) and quantum covariance (b), and experimental  $\text{KCuF}_3$  data at 6K. For comparison, the QMC result for  $\text{KCuF}_3$   $J_\perp$  is also shown in (b). Note the  $r > 10$  experimental values are systematically smaller than the theoretical 1D calculations as a consequence of finite interchain coupling  $J_\perp$ .

- [org/doi/10.1103/PhysRevB.103.224434](https://doi.org/10.1103/PhysRevB.103.224434).
- [65] S. R. White, Phys. Rev. Lett. **69**, 2863 (1992), URL <https://link.aps.org/doi/10.1103/PhysRevLett.69.2863>.
  - [66] S. R. White, Phys. Rev. B **48**, 10345 (1993), URL <https://link.aps.org/doi/10.1103/PhysRevB.48.10345>.
  - [67] A. E. Feiguin and S. R. White, Phys. Rev. B **72**, 220401(R) (2005), URL <https://link.aps.org/doi/10.1103/PhysRevB.72.220401>.
  - [68] T. Barthel, U. Schollwöck, and S. R. White, Phys. Rev. B **79**, 245101 (2009), URL <https://link.aps.org/doi/10.1103/PhysRevB.79.245101>.
  - [69] G. Alvarez, Comp. Phys. Comms. **180**, 1572–1578 (2009), URL <https://doi.org/10.1016/j.cpc.2009.02.016>.
  - [70] T. D. Kühner and S. R. White, Phys. Rev. B **60**, 335 (1999), URL <https://link.aps.org/doi/10.1103/PhysRevB.60.335>.
  - [71] A. Nocera and G. Alvarez, Phys. Rev. E **94**, 053308 (2016), URL <https://link.aps.org/doi/10.1103/PhysRevE.94.053308>.

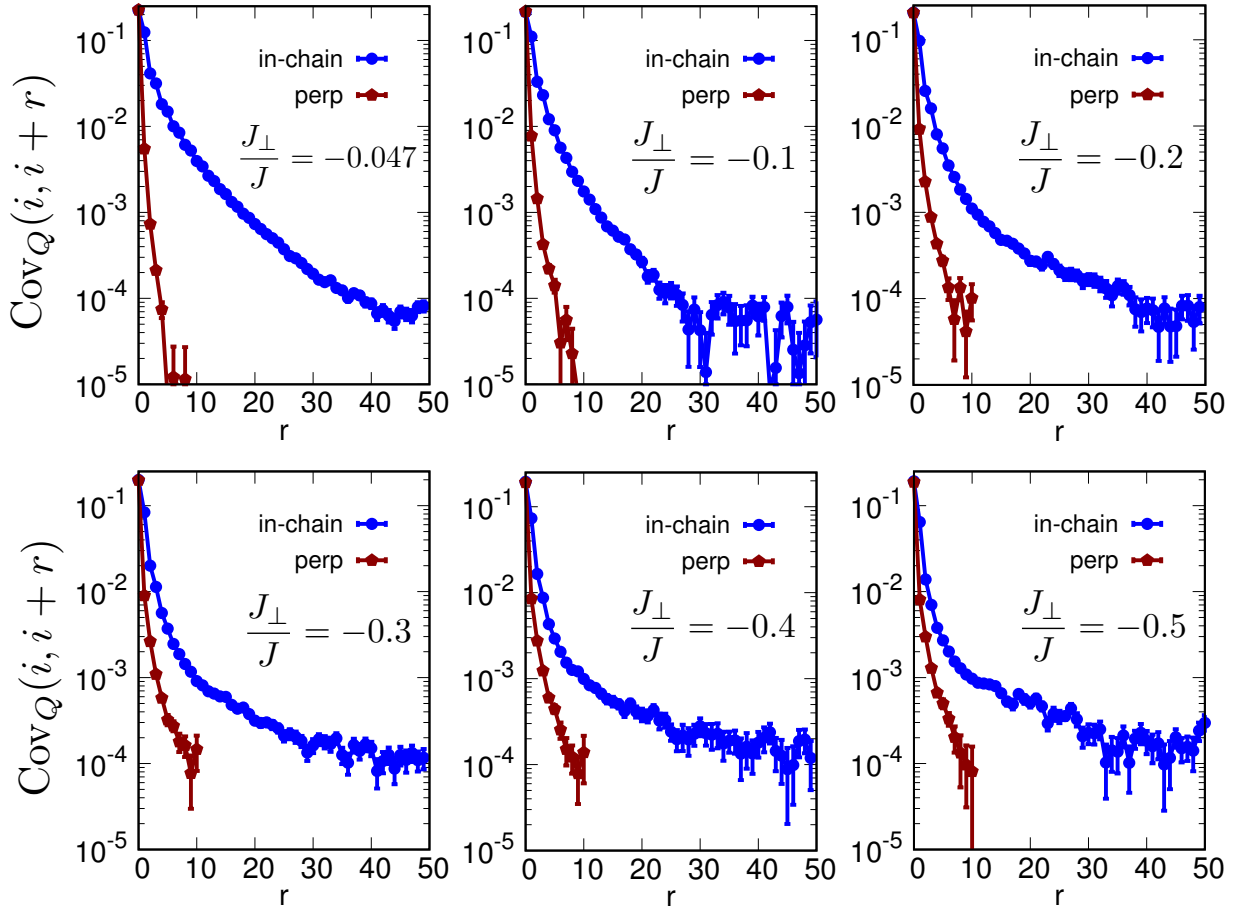


FIG. S4. **Dependence of  $\text{Cov}_Q$  on  $J_\perp$ .** Dependence of the quantum covariance on the ferromagnetic interchain coupling  $J_\perp$  for  $J_\perp/J = -0.047$  (as for  $\text{KCuF}_3$ ),  $-0.1$ ,  $-0.2$ ,  $-0.4$  and  $-0.5$ , at a temperature  $T/k_B = 6J/388$  (corresponding to 6K for  $\text{KCuF}_3$ ). The panels show QMC data obtained for a system with size  $100 \times 20 \times 20$ . Each panel shows the in-chain correlations ( $\text{Cov}_Q(i, i+x)$ , taking  $x$  as the lattice direction parallel to the chains) and the correlations perpendicular to the chain (e.g.  $\text{Cov}_Q(i, i+y)$ ).

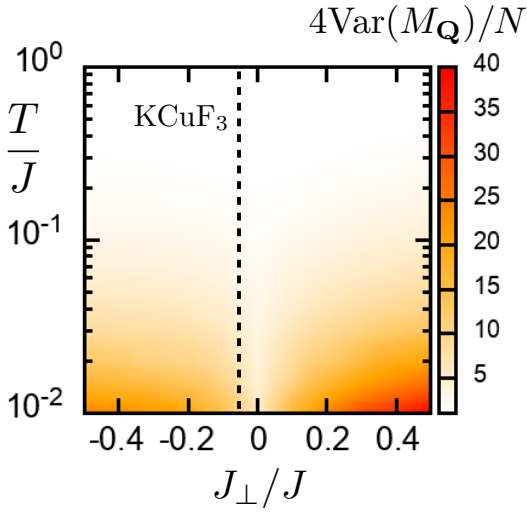


FIG. S5. **Quantum variance density of the order parameter for coupled Heisenberg chains.** The ordering vector  $\mathbf{Q}$  is  $(\pi, 0, 0)$  for  $J_\perp < 0$  and  $(\pi, \pi, \pi)$  for  $J_\perp > 0$ .